

A Toffoli Gadget for Magnetic Tunnel Junctions Boltzmann Machines

Dairong Chen,¹ Augustin Couton Wyporek,^{1,2} Pierre Chailloleau,² Ahmed Sidi El Valli,¹ Flaviano Morone,¹ Stephane Mangin,² Jonathan Z. Sun,³ Dries Sels,^{1,4} and Andrew D. Kent¹

¹*Center for Quantum Phenomena, Department of Physics,
New York University, New York, NY 10003 USA*

²*Université de Lorraine, CNRS, Institut Jean Lamour, F-54000 Nancy, France*

³*IBM T. J. Watson Research Center, Yorktown Heights, NY 10598, USA*

⁴*Center for Computational Quantum Physics, Flatiron Institute, New York, NY, USA*

Magnetic Tunnel Junctions (MTJs) are of great interest for non-conventional computing applications. The Toffoli gate is a universal reversible logic gate, enabling the construction of arbitrary boolean circuits. Here, we present a proof-of-concept construction of a gadget which encodes the Toffoli gate's truth table into the ground state of coupled uniaxial nanomagnets that could form the free layers of perpendicularly magnetized MTJs. This construction has three input bits, three output bits, and one ancilla bit. We numerically simulate the seven macrospins evolving under the stochastic Landau–Lifshitz–Gilbert (s-LLG) equation. We investigate the effect of the anisotropy-to-exchange-coupling strength ratio H_A/H_{ex} on the working of the gadget. We find that for $H_A/H_{\text{ex}} \lesssim 0.93$, the spins evolve to the Toffoli gate truth table configurations under LLG dynamics alone, while higher H_A/H_{ex} ratios require thermal annealing due to suboptimal metastable states. Under our chosen annealing procedure, the s-LLG simulation with thermal annealing achieves a 100% success rate up to $H_A/H_{\text{ex}} \simeq 3.0$. The feasibility of constructing MTJ-free-layer-based Toffoli gates highlights their potential in designing new types of MTJ-based circuits.

I. INTRODUCTION

Magnetic tunnel junctions (MTJs) hold significant potential in advancing future computing technologies. Traditionally, MTJs have been employed in the development of long-term storage elements and magnetic random access memory (MRAM). These applications utilize the stable and non-volatile characteristics of MTJs to store data efficiently and reliably [1, 2]. On the other hand, the stochastic behavior and dynamic nature of MTJs have led to novel computing applications beyond data storage [3]. With the rapid advances in machine learning and artificial intelligence, neuromorphic computing has emerged as a promising approach to meet the increasing demand for hardware capable of handling large-scale data processing, resolving the memory bottleneck issue, and having less energy consumption [4, 5]. MTJs have been shown to be a prominent candidate in the development of neuromorphic computing hardware [6–9].

MTJs also provide novel avenues for solving optimization problems. Probabilistic Ising machines built using MTJs have been used to find approximate solutions to NP-hard problems by encoding the true solution in the system's ground state [10–12]. Recently, several of the authors of this article conducted numerical studies to benchmark the performance of Landau-Lifshitz-Gilbert (LLG) dynamical systems in solving combinatorial optimization problems [13]. This work demonstrated that the stochastic and nonlinear dynamics governed by the stochas-

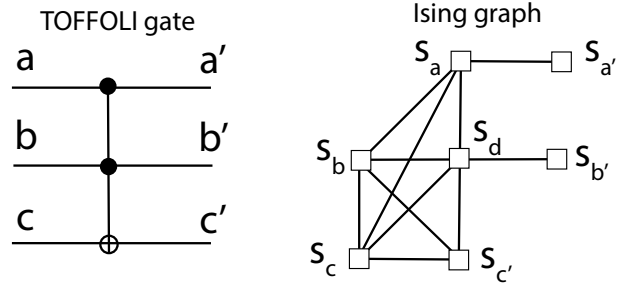


FIG. 1. The circuit representation of Toffoli gate (left) and an Ising spins network for the construction of a Toffoli gate (right) [14].

tic LLG equation has the potential to find better solutions to NP problems as system size scales up [13].

Building on these insights, we aim to broaden the scope of these unconventional computing application of MTJs. Although some combinatorial optimization problems, such as 3-SAT, are NP-complete and thus universal for computation, it can be quite cumbersome to encode the problem of interest into one of these Boolean satisfiability problems. It would be useful to be able to efficiently encode simple tasks, such as addition, multiplication or other basic operations into these unconventional dynamical systems. On the most general level, it suffices to encode a universal (reversible) logical gate into the ground state of some coupled MTJs. Here we focus on the Toffoli gate, which is a universal reversible gate [15] that

can serve as the building block for arithmetic operations. In the field of magnetism, efforts have been made to develop the Toffoli gate using three interacting classical spins [16], skyrmions [17, 18], and spin waves [19]. In this paper, we model the construction of a classical Toffoli gate using seven coupled uniaxial nanomagnets, which could represent the free layers of seven perpendicularly magnetized MTJs. We use the macrospin approximation for each free layer and apply LLG dynamics to simulate their evolution.

In the following sections, we will discuss our methods and results in detail. We begin by describing the mapping of the Toffoli gate's truth table to the ground state of an Ising Hamiltonian. Next, we outline our approach to simulating the macrospin model using the stochastic Landau-Lifshitz-Gilbert (sLLG) equation and discuss how macrospins can emulate Ising spins. We then detail our method for using coupled macrospins to construct a Toffoli gate. Finally, we present the results of our macrospin Toffoli gate simulations, both at zero temperature and using simulated annealing.

II. METHODS

A. Toffoli Gate Construction

The truth table of the Toffoli gate is described by the following Boolean function:

$$\{a, b, c\} \rightarrow \{a, b, c \oplus (a \wedge b)\}. \quad (1)$$

That is, the last bit flips conditional on the first two bits being 1. (It can be considered a '2'-controlled-NOT gate.) This gate is universal, as $\{a, b, 1\}$ will result in NAND of the inputs a and b , *i.e.*, $\{a, b, \neg(a \wedge b)\}$ and the NAND gate is a universal digital logic gate. Since the truth table can be represented as a permutation matrix, the Toffoli gate is also reversible.

This truth table of the Toffoli gate can be mapped to the ground states of a seven-coupled Ising spin system as shown in Chamon *et al.* [14]. We denote the Ising spins as s , which can only take two values $s = \pm 1$. The connection network between Ising spins is depicted in Fig. 1. In this system, we denote the spins that act as inputs s_a, s_b, s_c , the spin that acts as an ancilla s_d , and the spins that act as the outputs as $s_{a'}, s_{b'}, s_{c'}$. The Hamiltonian for this Toffoli gate construction is given by [14]

$$H_T = - \sum_{\langle i, j \rangle} J_{ij} s_i s_j - \sum_i h_i s_i, \quad (2)$$

where the J_{ij} is the coupling term between spins i and j , and h_i is the local field term applied to each

individual spin. The values for J_{ij} and h_i are shown in Table I.

s_a	s_b	s_c	s_d	$s_{a'}$	$s_{b'}$	$s_{c'}$	
-1	3	2	-4	1	0	-2	s_a
3	3	-4	8	0	1	4	s_b
2	-4	2	6	0	0	4	s_c
-4	8	6	-4	0	0	-6	s_d
1	0	0	0	0	0	0	$s_{a'}$
0	1	0	0	0	0	0	$s_{b'}$
-2	4	4	-6	0	0	-2	$s_{c'}$

TABLE I. J_{ij} -coupling between the input spins $\{s_a, s_b, s_c\}$, output $\{s_{a'}, s_{b'}, s_{c'}\}$ and the ancilla s_d . The diagonal represents the external field h_i applied on the i^{th} spin.

The Ising spins can only take two values: $s = \pm 1$, where $s = +1$ corresponds to logical 1, and $s = -1$ corresponds to logical 0. We denote logical input as a, b, c , logical ancilla as d , and logical output as a', b', c' . For simplicity, the configuration of the system is denoted as a binary string (a, b, c, d, a', b', c') , and we label each configuration by the decimal value of this binary string. For example, an input 001, an ancilla 0, and an output 001 form the binary string $(0, 0, 1, 0, 0, 0, 1)$, which corresponds to 17 in decimal representation. With this convention, we plot the energy landscape of the Hamiltonian H_T for different configurations in Fig. 2. The configurations with the lowest energies correspond to the correct input-output relations for the Toffoli gate's truth table.

Given the Toffoli gate Hamiltonian H_T , we model a system of 7 coupled single-domain ferromagnets that represent the 7 Ising spins. The macrospin approximation is applied to each domain such that the magnetization of the spins in the i^{th} domain are represented by one giant magnetic moment $\vec{m}_i = m_i \cdot \hat{m}_i$, with magnitude m_i and unit direction vector \hat{m}_i . This giant magnetic moment \vec{m}_i is referred to as a macrospin. We denote the macrospin system as $(\vec{m}_a, \vec{m}_b, \vec{m}_c, \vec{m}_d, \vec{m}_{a'}, \vec{m}_{b'}, \vec{m}_{c'})$. In contrast to Ising spins that are either up or down, a macrospin \vec{m} is defined on the surface of a 3D sphere with two degrees of freedom (in spherical coordinates, θ and ϕ), and evolves according to the LLG equation.

To emulate Ising spins using macrospins that follow full classical LLG dynamics, we include a uniaxial magnetic anisotropy along the \hat{z} -axis, such that the macrospins favor aligning up or down along the \hat{z} -axis. We initialize the system by converting $s = \pm 1$ to $\vec{m} = \pm m \cdot \hat{z}$, aligning the macrospin with the north or south pole based on the sign of the Ising spin. The three macrospins that act as the input

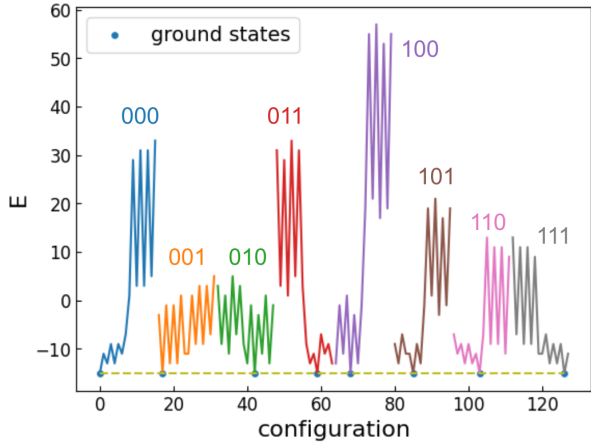


FIG. 2. The energy landscape calculated from the Hamiltonian H_T . The x axis represents the decimal representation of the binary string (a, b, c, d, a', b', c') and the y axis is the energy calculated from H_T by converting each logical bits to its corresponding Ising spins. Each color represents a set of configurations with the same fixed input values (a, b, c) . The blue dots represent the eight configurations with the lowest energies, which have the correct input-output relation according to the truth table for the Toffoli gate. The unit of energy will be taken to be $k_B T_{\text{amb}}$, where k_B is the Boltzmann constant and $T_{\text{amb}} = 300$ K, in the stochastic macrospin model discussed in Secs. II C and III B.

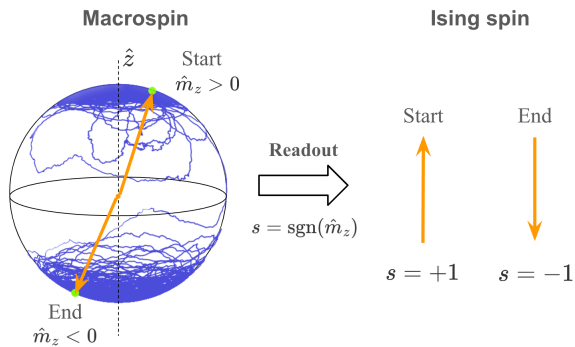


FIG. 3. Illustration of macrospin dynamics (left) and its mapping to an Ising spin (right).

of the Toffoli gate, $(\vec{m}_a, \vec{m}_b, \vec{m}_c)$, are fixed numerically to their initial states throughout the simulation, while the other four macrospins $(\vec{m}_d, \vec{m}_{a'}, \vec{m}_{b'}, \vec{m}_{c'})$ undergo LLG evolution. For readout at the end of the simulation, the sign of the projection of the macrospin's moment on the z-axis ($\text{sgn}(\hat{m}_z)$) is the binary value of Ising spin, as illustrated in Fig. 3.

B. LLG and s-LLG Equations

To describe the LLG dynamics that each macrospin follows, we begin by considering the micromagnetic energy of the system, E , which consists of three contributions:

$$E = E_{\text{ex}} + E_{\text{anis}} + E_Z, \quad (3)$$

where E_{ex} is the exchange energy between each pair of moments, E_{anis} is the anisotropic energy arising from the crystallographic structure of the domain, and E_Z is the Zeeman energy from an external field applied to the moment. The expression for each term is given by:

$$E_{\text{ex}} = -\mu_0 \sum_{\langle i, j \rangle} 2J_{ij} H_{\text{ex}} \frac{\vec{m}_i \cdot \vec{m}_j}{m_i + m_j}, \quad (4)$$

$$E_{\text{anis}} = -\frac{1}{2} \mu_0 \sum_i^n H_{A_i} m_i (\hat{e}_{hi} \cdot \hat{m}_i)^2, \quad (5)$$

$$E_Z = -\mu_0 \sum_i^n \vec{m}_i \cdot h_i H_{\text{ext}} \hat{e}_{\text{ext}i}, \quad (6)$$

where μ_0 is the vacuum permeability, J_{ij} are dimensionless coupling terms characterizing the exchange interaction between magnetic moments, and H_{ex} (with units of field) characterizes the general scale of the exchange coupling strength. The summation over $\langle i, j \rangle$ is over pairs of connected spins. H_{A_i} characterizes the magnetic anisotropy of moment i , and \hat{e}_{hi} is the unit vector representing the preferred crystallographic direction of moment i , which we set $\hat{e}_{hi} = \hat{z}$ to facilitate readout along this axis. h_i are dimensionless terms that characterize the external magnetic field applied to each magnetic moment, and H_{ext} (with units of field) characterize the general scale of the external field strength. $\hat{e}_{\text{ext}i}$ is the unit vector in the direction of the applied external field. We set $\hat{e}_{\text{ext}i} = \hat{z}$, so that this field is along the same axis as the magnetic anisotropy.

The i^{th} magnetic moment experiences an effective field $\vec{H}_{\text{eff},i}$, which can be obtained by computing the derivative of the micromagnetic energy E with respect to the magnetic moment \vec{m}_i :

$$\vec{H}_{\text{eff},i} = -\frac{1}{\mu_0} \frac{\partial E}{\partial \vec{m}_i}. \quad (7)$$

The expression for $\vec{H}_{\text{eff},i}$ is substituted into LLG equation, which determines the dynamical evolution of each magnetic moment at each time t :

$$\frac{d\vec{m}_i}{dt} = \gamma' \vec{m}_i \times \vec{H}_{\text{eff},i} - \frac{\alpha_i}{m_i} \vec{m}_i \times \frac{d\vec{m}_i}{dt}, \quad (8)$$

where $\gamma' = \mu_0\gamma$, γ is the gyromagnetic ratio. α_i is the damping constant of the i^{th} moment.

To account for the stochastic nature of the system under thermal fluctuations, a Langevin field term $\vec{H}_{\text{th},i}$ is added to the effective field $\vec{H}_{\text{eff},i}$:

$$\vec{H}_{\text{eff},i} \rightarrow \vec{H}_{\text{eff},i} + \vec{H}_{\text{th},i}. \quad (9)$$

The Langevin fields at times t and t' follow the statistical properties described in Refs. [20–22]:

$$\langle \vec{H}_{\text{th},i} \rangle = 0, \quad (10)$$

$$\langle \vec{H}_{\text{th},i,m}(t)\vec{H}_{\text{th},i,n}(t') \rangle = C_i\delta_{mn}\delta(t-t'), \quad (11)$$

$$C_i = \frac{2\alpha_i k_B T}{\mu_0^2 m_i \gamma (1 + \alpha_i^2)}, \quad (12)$$

where m and n represent the x, y, z components of the random field, and δ_{mn} and $\delta(t-t')$ are the Kronecker and Dirac delta functions respectively. t and t' denote different time instances, k_B is the Boltzmann constant, and T is the temperature. By integrating Eq. (11) over the discretized time step Δt , we can derive the standard deviation of $\vec{H}_{\text{th},i}$ in the x, y, z directions:

$$\sigma_i = \frac{1}{\mu_0} \sqrt{\frac{2\alpha_i k_B T}{m_i \gamma (1 + \alpha_i^2) \Delta t}}. \quad (13)$$

For each component x, y, z of $\vec{H}_{\text{th},i}$, we sample a value from a Gaussian distribution with a mean $\mu = 0$ and standard deviation given by σ_i from Eq. (13).

For the numerical integration, we use the Stratonovich interpretation of the stochastic process and implement Heun's method as our integration scheme. In the study by Ament *et al.* [23], Heun's integration scheme converges to the Stratonovich solution and preserves the norm of \hat{m}_i for small time steps when simulating s-LLG dynamics.

C. Implementation of Toffoli Gate Hamiltonian

In our simulation, we assume identical parameters for all n macrospins, allowing us to omit the index i for the following quantities: $H_{A_i} = H_A$, $\alpha_i = \alpha$, and $m_i = m$. This approach models an array of perfectly identical macrospins. The simulation can then be simplified to focus solely on the evolution of the unit magnetic moment \hat{m}_i , as shown by the blue \hat{m} trajectories in Fig. 3. The energy terms can thus be

simplified as follows:

$$E_{\text{ex}} = -\mu_0 m H_{\text{ex}} \sum_{\langle i,j \rangle}^n J_{ij} (\hat{m}_i \cdot \hat{m}_j), \quad (14)$$

$$E_{\text{anis}} = -\frac{1}{2} \mu_0 m H_A \sum_i^n (\hat{m}_i \cdot \hat{z})^2, \quad (15)$$

$$E_Z = -\mu_0 m H_{\text{ext}} \sum_i^n h_i (\hat{m}_i \cdot \hat{z}). \quad (16)$$

The Toffoli gate Hamiltonian H_T can be directly mapped to the system's micromagnetic energy terms E_{ex} and E_Z . Specifically, the J_{ij} terms in H_T in Eq. (2) correspond to the J_{ij} terms in E_{ex} in Eq. (14), and the h_i terms in H_T correspond to the h_i terms in E_Z in Eq. (16). To maintain the relative strength between the coupling terms and the local field terms as given by H_T , we set the general scale of the exchange coupling strength H_{ex} equal to the local field strength H_{ext} , *i.e.*, $H_{\text{ex}} = H_{\text{ext}}$ for all trials.

The ratio of anisotropy H_A to coupling strength H_{ex} influences the quality of the final output. High anisotropy causes spins to align more strictly along the north and south poles, emulating binary Ising spins. However, high anisotropy also makes it more difficult for spins to overcome the energy barrier to flip, increasing the likelihood that the system will be trapped in configurations that are not consistent with the truth table of the Toffoli gate. Conversely, if H_A is relatively small, the spins can flip more easily, but this can result in the spins not aligning well with the z -axis, complicating the read-out process. In addition, thermal effects play a role in reaching the correct ground state when simulated annealing is incorporated. High temperatures produce thermal fluctuations that allow spins to overcome energy barriers and eventually find the ground state through annealing.

Considering the many possible contributing factors, we simulate the zero-temperature dynamics and the dynamics with thermal annealing separately. First, we investigate the ability of pure (*i.e.*, zero temperature) LLG dynamics to find the correct configurations given by the truth table as a function of H_A/H_{ex} , with $H_{\text{ex}} = H_{\text{ext}}$ fixed. The values of the parameters for our simulation are shown in Table II. The values are realistic for the free layers of perpendicularly magnetized magnetic tunnel junction nanopillars [1].

In addition, we study the ability of combined stochastic LLG dynamics with simulated annealing to reach the true ground state as a function of H_A/H_{ex} . We have empirically chosen an annealing schedule that decreases from $T = 300$ to 0K over 150 evenly

spaced steps. We set the exchange field H_{ex} such that the exchange energy E_{ex} is the order $k_B T_{\text{amb}}$, with $T_{\text{amb}} = 300$ K. This ensures the system has sufficient thermal energy to overcome energy barriers as it evolves. At each temperature, we let the system evolve with 10^5 iterations, which corresponds to $1\mu\text{s}$ in physical units. This time is longer than a typical spin relaxation time. For instance, considering spin relaxation in the exchange field, $t_{\text{relax}} \approx 2\pi/(\alpha\mu_0\gamma H_{\text{ex}}) \approx 0.1\mu\text{s}$, which is one order magnitude smaller than $1\mu\text{s}$. Therefore, our system will be in or very close to thermal equilibrium with the environment at the end of each temperature step.

Damping Constant	α	0.01
Magnetic Moment	m	8×10^{-19} J/T
Ambient Temperature	T_{amb}	300K
Exchange Field	H_{ex}	4.12×10^3 A/m
Simulation Time Step	Δt	0.01 ns
Iterations at Each Temperature		1×10^5
Iterations at 0K (LLG)		5×10^5

TABLE II. Values of the parameters chosen for simulation.

III. RESULTS

A. Zero temperature simulations

We first simulate the construction of a Toffoli Gate using LLG dynamics at zero temperature ($T = 0$ K). For a given initial configuration (a, b, c, d, a', b', c') , we begin by initializing the macrospins to the corresponding values $(\hat{m}_a, \hat{m}_b, \hat{m}_c, \hat{m}_d, \hat{m}_{a'}, \hat{m}_{b'}, \hat{m}_{c'})$. The input bits (a, b, c) are converted into macrospins $(\hat{m}_a, \hat{m}_b, \hat{m}_c)$ by aligning them strictly along the \hat{z} axis, with bit 0 corresponding to $-\hat{z}$ and bit 1 to $+\hat{z}$. Then these three macrospins are numerically fixed throughout the simulation. We initialize the output bits (d, a', b', c') as $(\hat{m}_d, \hat{m}_{a'}, \hat{m}_{b'}, \hat{m}_{c'})$ by first aligning these vectors along the z axis. Then we add a small angular deviation of 0.01 rad from \hat{z} to prevent the spins from experiencing zero initial torque (*i.e.*, to avoid the cross-product terms in Eq. (8) being zero).

For each Toffoli Gate input (a, b, c) , there are 16 different possible initial configurations of (d, a', b', c') . For a fixed input (a, b, c) , we run 16 trials with different initial conditions of (d, a', b', c') , allowing the system to evolve to its final state. We record the final state and count the number of trials that result in an output (a', b', c') consistent with the Toffoli gate truth table and use this to compute the success rate.

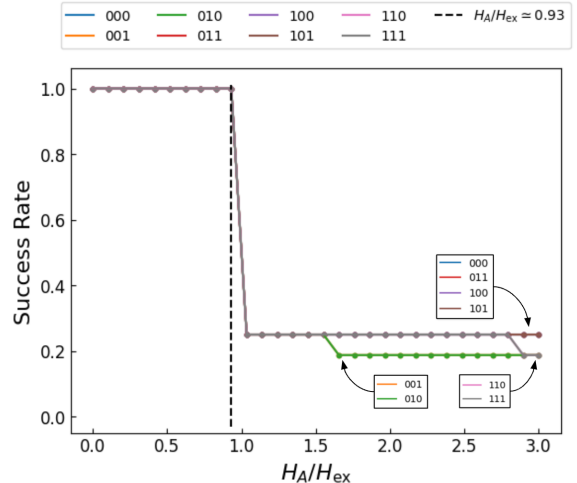


FIG. 4. Success rate of the Toffoli gate reaching the correct output as a function of H_A/H_{ex} ratio, under deterministic (zero temperature) LLG dynamics. The results for each input (a, b, c) are color-coded in the plot. The graph appears to have fewer colors than listed due to multiple overlapping lines stacked on top of each other. The black dashed line at $H_A/H_{\text{ex}} \approx 0.93$ represents the largest H_A/H_{ex} in our simulation that still achieves a 100% success rate for all trials.

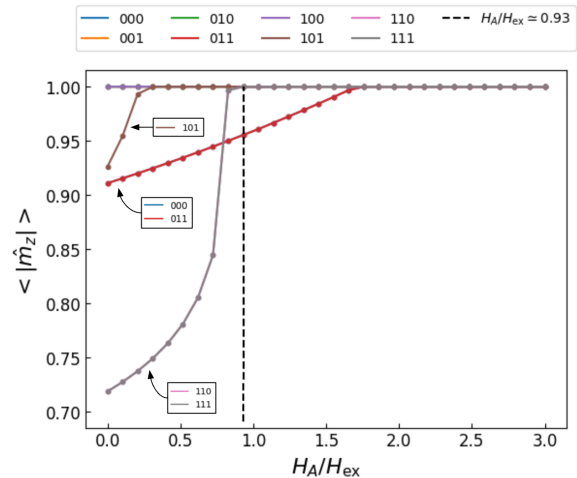


FIG. 5. Average \hat{z} projection of output spins $\langle |\hat{m}_z| \rangle$ as a function of H_A/H_{ex} ratio, under deterministic (zero temperature) LLG dynamics. The results for each input configuration (a, b, c) are color-coded in the plot. The graph appears to have fewer colors than listed due to multiple overlapping lines stacked on top of each other. The black dashed line at $H_A/H_{\text{ex}} \approx 0.93$ represents the largest H_A/H_{ex} in our simulation that still achieves a 100% success rate for all trials.

The process is repeated for different H_A/H_{ex} ratios, and the result is shown in Fig. 4. We observe a 100%

success rate of reaching the correct configuration for $H_A/H_{\text{ex}} \lesssim 0.93$.

To assess how Ising-like the spins are at the end of the simulation, we record the absolute magnitude of the final \hat{z} projection $|\hat{m}_z| = |\hat{m} \cdot \hat{z}|$ for each output configuration $(\hat{m}_d, \hat{m}_{a'}, \hat{m}_{b'}, \hat{m}_{c'})$. There are 16 different trials for each input (a, b, c) , we take the average of $|\hat{m}_z|$ across both the four output spins and the 16 trials to obtain a single value. The results are shown in Fig. 5. Since we set the external field applied locally to each macrospin as $\hat{e}_{\text{ext}} = \hat{z}$, an Ising-like output is still observed even when $H_A = 0$, with the smallest $\langle |\hat{m}_z| \rangle = 0.72$. We also observe that as H_A/H_{ex} increases, $\langle |\hat{m}_z| \rangle$ approaches 1, which indicates that the spins are more Ising like as the anisotropy increases.

B. Simulation with thermal annealing (s-LLG)

In this section, we simulate the Toffoli gate construction with simulated annealing. We fix the exchange coupling strength such that E_{ex} between spins is on the order of $k_B T_{\text{amb}}$, where T_{amb} is the ambient temperature of 300K. For each Toffoli Gate input (a, b, c) , we start with the configuration $(a, b, c, 0, 0, 0, 0)$ and perform an annealing process from 300 to 0K over 150 evenly spaced steps. Since we start at high temperature, the system is able to visit different magnetic configurations. Therefore, it is not as necessary to initialize the system with different configurations (d, a', b', c') , as in the 0K case. After the annealing process, we record the final state and repeat the simulations for 500 independent trials. We do the same simulations for different ratios H_A/H_{ex} . The results are shown in Figs. 6 and 7.

With the assistance of simulated annealing, we observe that within the statistics of 500 trials, the system is able to achieve a 100% probability of finding the correct output for H_A/H_{ex} up to $H_A/H_{\text{ex}} \simeq 3.0$, which is higher than the limit of $H_A/H_{\text{ex}} \simeq 0.93$ observed with zero-temperature pure LLG dynamics. Further, at $H_A/H_{\text{ex}} \simeq 3.0$, the final configurations are all Ising-like, with all spins aligned along the z axis as shown in Fig. 7.

C. Conclusion

We have demonstrated a proof-of-concept Toffoli gate construction using macrospins with a uniaxial magnetic anisotropy that could be formed by the free magnetic layers of MTJs. Specifically, we investigated the influence of the ratio of the uniaxial magnetic anisotropy to the exchange coupling, H_A/H_{ex} ,

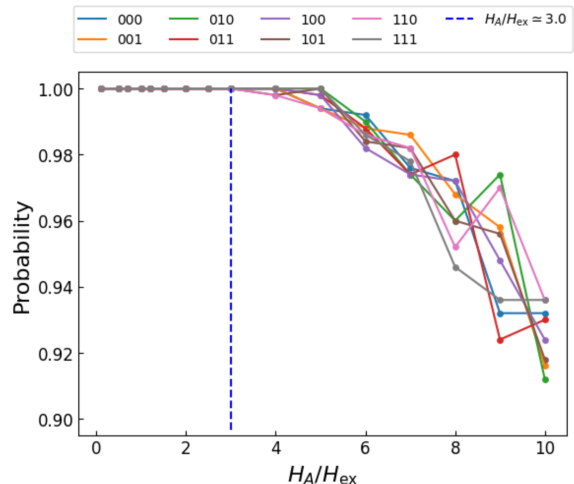


FIG. 6. Probability of reaching the correct configurations at different H_A/H_{ex} ratios for Toffoli gate construction with s-LLG dynamics and simulated annealing. The results for each (a, b, c) are color-coded in the plot. For each (a, b, c) , the simulation is repeated for 500 trials. Within the statistics of 500 trials, values above $H_A/H_{\text{ex}} \simeq 3.0$ fails to reach a 100% probability of producing the correct output, as shown by the blue dashed line.

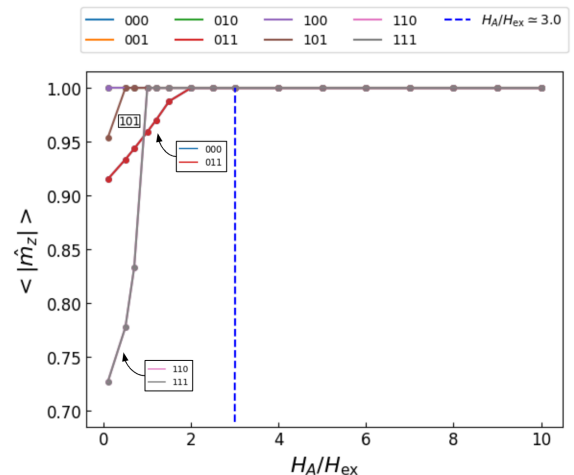


FIG. 7. Average \hat{z} projection of output spins, $\langle |\hat{m}_z| \rangle$, as a function of H_A/H_{ex} ratios for Toffoli gate construction with s-LLG dynamics and simulated annealing. The average is taken across 500 trials. The results for each (a, b, c) are color-coded in the plot. The blue dashed line at $H_A/H_{\text{ex}} \simeq 3.0$ represents the largest H_A/H_{ex} allowed to achieve a 100% probability of reaching the correct output with simulated annealing.

on the spin dynamics. Remarkably, the zero temperature LLG dynamics always ends in configurations consistent with the Toffoli gate's truth table provided that $H_A/H_{\text{ex}} \lesssim 0.93$. Introducing thermal anneal-

ing allows to push this ratio to higher values, up to $H_A/H_{\text{ex}} \simeq 3.0$, while keeping a 100% success rate.

Our modeling thus shows that a universal reversible gate can be constructed from interacting classical macrospins, highlighting a promising avenue for research with arrays of interacting MTJs [24–26]. Although our simulation has shown the feasibility of this approach, further research is needed. Specifically, this work explored the feasibility of constructing a single Toffoli gate. Future theoretical work could investigate the feasibility of building circuits using multiple Toffoli gates for real-world computational tasks. These would address the questions of methods, properties, and fidelity of connected Toffoli gates and, for example, how the time to solution

scales with the problem size.

Acknowledgement

The research at NYU was supported by the Office of Naval Research (ONR) under Award No. N00014-23-1-2771 and in part by the National Science Foundation (NSF) under Award DMR-2105114. Research at the University of Lorraine was supported by “MAT-PULSE,” part of the French PIA project “Lorraine Université d’Excellence” reference ANR-15-IDEX-04-LUE. This work was also supported in part through the NYU IT High Performance Computing resources, services, and staff expertise.

-
- [1] A. D. Kent and D. C. Worledge, A new spin on magnetic memories, *Nature Nanotechnology* **10**, 187 (2015).
- [2] J. Ender, S. Fiorentini, R. L. De Orío, W. Goes, V. Sverdlov, and S. Selberherr, Emerging CMOS Compatible Magnetic Memories and Logic, *IEEE Journal of the Electron Devices Society* **9**, 456 (2021).
- [3] G. Finocchio, J. A. C. Incorvia, J. S. Friedman, Q. Yang, A. Giordano, J. Grollier, H. Yang, F. Ciubar, A. V. Chumak, A. J. Naeemi, S. D. Cofana, R. Tomasello, C. Panagopoulos, M. Carpentieri, P. Lin, G. Pan, J. J. Yang, A. Todri-Sanial, G. Boschetto, K. Makasheva, V. K. Sangwan, A. R. Trivedi, M. C. Hersam, K. Y. Camsari, P. L. McMahon, S. Datta, B. Koiller, G. H. Aguilar, G. P. Temporão, D. R. Rodrigues, S. Sunada, K. Everschor-Sitte, K. Tatsumura, H. Goto, V. Puliafito, J. Åkerman, H. Takesue, M. D. Ventra, Y. V. Pershin, S. Mukhopadhyay, K. Roy, I.-T. Wang, W. Kang, Y. Zhu, B. K. Kaushik, J. Hasler, S. Ganguly, A. W. Ghosh, W. Levy, V. Roychowdhury, and S. Bandyopadhyay, Roadmap for unconventional computing with nanotechnology, *Nano Futures* **8**, 012001 (2024).
- [4] C. D. Schuman, S. R. Kulkarni, M. Parsa, J. P. Mitchell, P. Date, and B. Kay, Opportunities for neuromorphic computing algorithms and applications, *Nature Computational Science* **2**, 10 (2022).
- [5] W. Zhang, B. Gao, J. Tang, P. Yao, S. Yu, M.-F. Chang, H.-J. Yoo, H. Qian, and H. Wu, Neuro-inspired computing chips, *Nature Electronics* **3**, 371 (2020).
- [6] J. Torrejon, M. Riou, F. A. Araujo, S. Tsunegi, G. Khalsa, D. Querlioz, P. Bortolotti, V. Cros, K. Yakushiji, A. Fukushima, H. Kubota, S. Yuasa, M. D. Stiles, and J. Grollier, Neuromorphic computing with nanoscale spintronic oscillators, *Nature* **547**, 428 (2017).
- [7] M. Romera, P. Talatchian, S. Tsunegi, F. Abreu Araujo, V. Cros, P. Bortolotti, J. Trastoy, K. Yakushiji, A. Fukushima, H. Kubota, S. Yuasa, M. Ernault, D. Vodenicarevic, T. Hirtzlin, N. Locatelli, D. Querlioz, and J. Grollier, Vowel recognition with four coupled spin-torque nano-oscillators, *Nature* **563**, 230 (2018).
- [8] J. Grollier, D. Querlioz, K. Y. Camsari, K. Everschor-Sitte, S. Fukami, and M. D. Stiles, Neuromorphic spintronics, *Nature Electronics* **3**, 360 (2020).
- [9] D. Marković, A. Mizrahi, D. Querlioz, and J. Grollier, Physics for neuromorphic computing, *Nature Reviews Physics* **2**, 499 (2020).
- [10] K. Y. Camsari, R. Faria, B. M. Sutton, and S. Datta, Stochastic p-Bits for Invertible Logic, *Physical Review X* **7**, 031014 (2017).
- [11] W. A. Borders, A. Z. Pervaiz, S. Fukami, K. Y. Camsari, H. Ohno, and S. Datta, Integer factorization using stochastic magnetic tunnel junctions, *Nature* **573**, 390 (2019).
- [12] J. Si, S. Yang, Y. Cen, J. Chen, Y. Huang, Z. Yao, D.-J. Kim, K. Cai, J. Yoo, X. Fong, and H. Yang, Energy-efficient superparamagnetic Ising machine and its application to traveling salesman problems, *Nature Communications* **15**, 3457 (2024).
- [13] D. Chen, A. D. Kent, D. Sels, and F. Morone, Solving combinatorial optimization problems through stochastic Landau-Lifshitz-Gilbert dynamical systems (2024), arXiv:2407.00530.
- [14] C. Chamon, E. R. Mucciolo, A. E. Ruckenstein, and Z.-C. Yang, Quantum vertex model for reversible classical computing, *Nature Communications* **8**, 15303 (2017).
- [15] T. Toffoli, Reversible computing, in *Automata, Languages and Programming*, edited by J. de Bakker and J. van Leeuwen (Springer, Berlin, Heidelberg, 1980) pp. 632–644.

- [16] D. Nuzzi, L. Banchi, R. Vaia, E. Compagno, A. Cucoli, P. Verrucchi, and S. Bose, Full-magnetic implementation of a classical toffoli gate, *Phys. Rev. Res.* **6**, 013308 (2024).
- [17] J. I. Costilla, J. W. Alegre, A. Talledo, and B. R. Pujada, Implementation of the Toffoli and Peres reversible logic gates using magnetic skyrmions in operational gates, *Journal of Applied Physics* **134**, 013903 (2023).
- [18] M. Chauwin, X. Hu, F. Garcia-Sanchez, N. Betrabet, A. Paler, C. Moutafis, and J. S. Friedman, Skyrmion Logic System for Large-Scale Reversible Computation, *Physical Review Applied* **12**, 064053 (2019).
- [19] M. Balynskiy, H. Chiang, D. Gutierrez, A. Kozhevnikov, Y. Filimonov, and A. Khitun, Reversible magnetic logic gates based on spin wave interference, *Journal of Applied Physics* **123**, 144501 (2018).
- [20] W. F. Brown, Thermal Fluctuations of a Single-Domain Particle, *Physical Review* **130**, 1677 (1963).
- [21] D. V. Berkov, Magnetization Dynamics Including Thermal Fluctuations: Basic Phenomenology, Fast Remagnetization Processes and Transitions Over High-energy Barriers, in *Handbook of Magnetism and Advanced Magnetic Materials* (John Wiley & Sons, Ltd, 2007).
- [22] J. L. García-Palacios and F. J. Lázaro, Langevin-dynamics study of the dynamical properties of small magnetic particles, *Phys. Rev. B* **58**, 14937 (1998).
- [23] S. Ament, N. Rangarajan, A. Parthasarathy, and S. Rakheja, Solving the stochastic landau-lifshitz-gilbert-slonzewski equation for monodomain nanomagnets : A survey and analysis of numerical techniques (2017), arXiv:1607.04596.
- [24] P. Talatchian, M. W. Daniels, A. Madhavan, M. R. Pufall, E. Jué, W. H. Rippard, J. J. McClelland, and M. D. Stiles, Mutual control of stochastic switching for two electrically coupled superparamagnetic tunnel junctions, *Physical Review B* **104**, 054427 (2021).
- [25] N.-T. Phan, L. Soumah, A. Sidi El Valli, L. Hutin, L. Anghel, U. Ebels, and P. Talatchian, Electrical Coupling of Perpendicular Superparamagnetic Tunnel Junctions for Probabilistic Computing, in *Proceedings of the 17th ACM International Symposium on Nanoscale Architectures* (ACM, Virtual OR USA, 2022) pp. 1–6.
- [26] L. Schnitzspan, M. Kläui, and G. Jakob, Electrical coupling of superparamagnetic tunnel junctions mediated by spin-transfer-torques, *Applied Physics Letters* **123**, 232403 (2023).